Basics of QCD for the LHC: $pp \to H + X$ as a case study

Fabio Maltoni
Centre for Cosmology, Particle Physics and Phenomenology (CP3)
Université Catholique de Louvain, Chemin du Cyclotron 2, B-1348 Louvain-la-Neuve, Belgium

Abstract
Quantum Chromo Dynamics (QCD) provides the theoretical framework for any study of TeV scale physics at LHC. Being familiar with the basic concepts and techniques of QCD is therefore a must for any high-energy physicist. In these notes we consider Higgs production via gluon fusion as an example on how accurate and flexible predictions can be obtained in perturbative QCD. We start by illustrating how to calculate the total cross section at the leading order (yet one loop) in the strong coupling α_S and go through the details of the next-to-leading order calculation eventually highlighting the limitations of fixed-order predictions at the parton level. Finally, we briefly discuss how more exclusive (and practical) predictions can be obtained through matching/merging fixed-order results with parton showers.

1 Introduction

Strongly interacting particles can be described in terms of a $SU(3)$ gauge theory field theory involving gluons and quarks:

$$\mathcal{L}_{\rm QCD} = -\frac{1}{4} G^{\mu\nu,a} G^a_{\mu\nu} + \sum_f \bar{\psi}^f_i \, i \not{D}_{ij} \, \psi^f_j \,, \tag{1}$$

where the sum runs over the quark flavors,

$$\begin{aligned} G^a_{\mu\nu} &= \partial_\mu A^a_\nu - \partial_\nu A^a_\mu - g_s f^{abc} A^b_\mu A^c_\nu \,, \\ D_{\mu,ij} &= \partial_\mu \delta_{ij} + i g_s t^a_{ij} A^a_\mu \,, \end{aligned}$$

and t^a_{ij} are the Gell-Mann matrices in the fundamental representation and f^{abc} are the structure functions of SU(3), with

$$[t^a, t^b] = i f^{abc} t^c \,. \tag{2}$$

Notwithstanding its apparent simplicity, QCD is an amazingly rich theory which is able to account for a wide diversity of phenomena, ranging from really strong (non-perturbative) interactions at low scales, below 1 GeV, to rather weak (perturbative) interactions up to scales of the TeV at colliders, from low density to high density states such as those happening in nuclei collisions or inside stars, from low to high temperatures. For proton-proton collisions at the LHC, where one can consider zero temperature and density, QCD is complicated enough that we have no means available (for the moment!) to solve it exactly and we have to resort to a variety of approximate methods, including perturbation theory (when the coupling is small) and lattice calculations (when the coupling is large). Thanks to the work of theoretical and experimental physicists over the last fourty years we are convinced that QCD is a good theory of the strong interactions, of course in the range of energies explored so far and to the level of the theoretical accuracy that can be achieved with current technologies.

There are many excellent references on QCD with applications to collider physics, from books, (e.g., [1]) to review articles, to write-up of lectures given in schools, and in particular some of those given at the CERN schools over the years. My lectures at the school were largely based on the inspiring ones by Michelangelo Mangano [2], Paolo Nason [3] and on the most recent ones by Gavin Salam [4],

which I warmly reccommend. In these notes, I'll present a case study, i.e. how QCD can make accurate predictions for Higgs production in gluon fusion at the LHC. The aim is to see the basic concepts at work for a realistic and very important process so to verify their understanding and also to have a closer look at the basic techniques used to perform such calculations. When needed and to avoid repetitions, I will refer to specific sections of Ref. [4] as [QCD: Section number] where the reader will find further information on the basic concepts. Links to simple Mathematica® notebooks with the calculations described below can be found at `http://maltoni.home.cern.ch/`.

2 Higgs cross section at the LHC

The factorisation theorem states that the total cross section for the inclusive production of Higgs at the LHC can be written as [1]

$$\sigma(H+X) = \Sigma_{i,j} \int dx_1 f_i(x_1,\mu_F) \int dx_2 f_j(x_2,\mu_F) \times \hat{\sigma}_{ij\to H+x}(s, m_H, \mu_F, \mu_R)\,, \tag{3}$$

where the $f_{i/j}(x,\mu_F)$ are the parton distributions functions (long distance term, non-perturbatively calculable) and $\hat{\sigma}$ is the partonic cross section (short distance term, calculable in perturbation theory).
$\hat{\sigma}$ can be written as an expansion in α_S:

$$\begin{aligned}\hat{\sigma}(ij\to H+x) &= \hat{\sigma}^{(0)}(ij\to H)\\ &+ \hat{\sigma}^{(1)}(ij\to H+\text{up to 1 parton})\\ &+ \hat{\sigma}^{(2)}(ij\to H+\text{up to 2 partons})\\ &+ \dots\end{aligned} \tag{4}$$

where the first term gives the leading order (LO) approximation and it is of order α_S^2, the second next-to-leading (NLO) order (α_S^3) and so on.

It is interesting to know how the Higgs predictions improved and evolved over time. The LO production was considered a long ago [5], the next-to-leading order (NLO) QCD corrections [6–9] were calculated decades ago in the so-called effective field theory (HEFT) approximation (which will be explained in the following) as well in the full SM and found to be very large ($\sigma^{\rm NLO}/\sigma^{\rm LO} \sim 2$). This motivated the formidable endeavour of the next-to-next-to-leading order (NNLO) QCD calculations, which have been fully evaluated in HEFT [10–12]. Given that corrections to the HEFT been estimated through a power expansion [13–16] and found to have a negligible impact on total rates, NNLO is the current state of the art for fixed-order predictions.

Before going into the details of the computation of the Higgs cross section, let us remind a few general important points that are relevant for any computation in QCD.

- At LO the factorisation theorem reduces to the parton model: the parton distribution functions $f_i(x)$ are just the probabilities (and therefore positive-definite) of finding a given parton in the initial state hadrons at a given resolution scale μ_F and $\hat{\sigma}$ gives the probability that such partons with a total energy $s = x_1 x_2 S$ will "fuse" into a Higgs.
- Total cross sections are the first and simplest example of a larger class of observables, called Infrared Safe (IS) quantities [QCD:2.3.2], which can be consistently computed in QCD and then compared to experimental data. Such quantities always need to be (at least to some degree) inclusive on possible extra radiation and in particular resilient under soft and/or collinear radiation. The

[1] Be careful here as for simplicity we adopt the usual pragmatic approach on Higgs production at the LHC and imagine it coming from different channels: gluon-gluon fusion, vector-boson-fusion, vector-boson-associated...and so on. We restrict the discussion to the first one which is the leading mechanism. In fact, various channels overlap if contributions are organized as powers of strong and weak couplings (e.g., $gg \to H$ appears at the same order in α_S and y_t as $gg \to t\bar{t}H$) and in general they mix-up once higher-order QCD and EW corrections are included. The separation into channels is anyway useful from the experimental point of view as they typically lead to different final state signatures.

most known example of IS quantities beyond total cross sections are jets [QCD:5]. The constraint of infrared safety becomes non-trivial already at NLO for Eq. (3).

- Total cross sections always inclusive of any possible extra QCD radiation in the event, hereby denoted by X, even when the calculation is performed at LO. In this case, extra radiation up to the scale μ_F is accounted for by the parton distribution function's (PDF), while hard radiation is consistently neglected being of higher order (α_S). Alternatively, one can prove that the total cross section for producing "just a Higgs", i.e., Higgs + no resolvable radiation at an arbitrary small scale is exactly zero at all orders in perturbation theory.
- A very important point to always keep in mind is that the the "adjectives" LO, NLO, NNLO need to be always referred to a specific observable, i.e. different observables in a given calculation can be predicted at a different order. For example, when talking about a "NNLO calculation for Higgs production in gluon fusion", what is really meant is that the total inclusive cross section is known at NNLO. The same calculation can predict the rate for Higgs+1 jet (inclusive and exclusive) at NLO and Higgs+2 jets only at LO (where exclusive and inclusive is the same).
- Beyond LO, the separation between long-distance and short-distance physics as described by μ_F (and also μ_R) becomes non-trivial. μ_F and μ_R represent arbitrary scales in the calculation, whose dependence is generated by the truncation of the perturbative expansion at a given order. Exploiting the fact that physical results must be independent on such scales one finds renormalisation-group type equations, such as the β function of QCD [QCD:1.2.3] and the so-called DGLAP evolution equations for the PDF's [QCD:3.2].
- The residual dependence of σ on μ_F and μ_R at any given order in perturbation theory is often used to gauge the accuracy of the predictions [QCD:4.4.1]. This is by itself a very crude approximation, while the towers of leading (subleading,...) log's of the scales can be predicted at all orders in perturbation theory, only an explicit computation is able to provide the finite terms at higher orders. In practice, it is common to choose central scales as the typical hard scale in a process and vary them independently between $1/2$ and 2 to identify an uncertainty. However, no solid and unique procedure exists to identify central reference values and variation intervals and to associate a confidence level. However, milder scale dependence of higher-order results compared to lower ones is always used to gauge the improvement on the accuracy of a given prediction.

3 $pp \to H + X$ at leading order

At LO Eq. 3 can be rewritten as

$$\sigma^{\rm LO}(H+X) = \int_{\tau_0}^1 dx_1 \int_{\tau_0/x_1}^1 dx_2 f_g(x_1,\mu_F) f_g(x_2,\mu_F) \times \hat{\sigma}^{(0)}(gg\to H)\,, \tag{5}$$

where $\tau_0 = m_H^2/S$ and $s = x_1 x_2 S$. $\hat{\sigma}$ for a $2 \to 1$ process can be rewritten as

$$\begin{aligned} \hat{\sigma} &= \frac{1}{2s}\overline{|\mathcal{A}|^2}\frac{d^3P}{(2\pi)^3 2E_H}(2\pi)^4\delta^4(p+q-P_H) \\ &= \frac{1}{2s}\overline{|\mathcal{A}|^2}2\pi\delta(s-m_H^2)\,, \end{aligned} \tag{6}$$

where

$$\tau \equiv x_1 x_2 = \frac{S}{s}, \qquad \tau_0 = \frac{m_H^2}{S}\,. \tag{7}$$

Performing the change of variables $x_1, x_2 \to \tau, y$ with $x_1 \equiv \sqrt{\tau}e^y$, $x_2 \equiv \sqrt{\tau}e^{-y}$ (verify that the jacobian J is equal to 1) the change of the integration limits and the result becomes

$$\sigma^{\rm LO}(H+X) = \frac{\pi\overline{|\mathcal{A}|^2}}{m_H^2 S}\int_{\log\sqrt{\tau_0}}^{-\log\sqrt{\tau_0}} dy\, x g(\sqrt{\tau_0}e^y) g(\sqrt{\tau_0}e^{-y})\,. \tag{8}$$

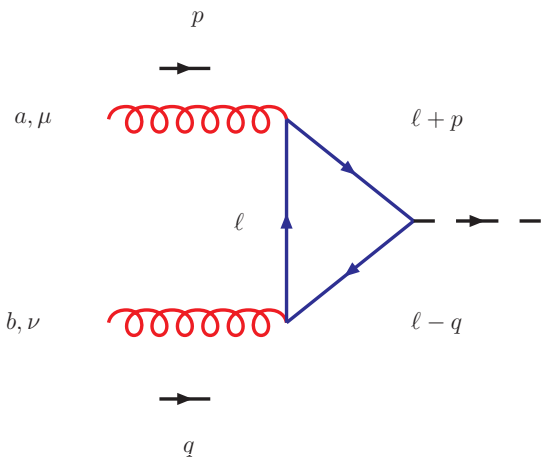

Figure 1: Representative Feynman diagram for the process $gg \to H$. Another diagram, the one with the gluons exchanged, contributes to the total amplitude.

This expression shows that for the cross section of a $2 \to 1$ process at LO, the contribution from the parton distributions (a quantity known as gluon-gluon luminosity) factorises from the dynamics ($|\mathcal{A}|^2$). The gluon-gluon luminosity depends only on the kinematics in the limits of integration and can be computed once for all for each Higgs mass. The problem is therefore reduced to the computation of the amplitude $\mathcal{A}$.

3.1 My first loop (yet finite!) amplitude: $gg \to H$

Being a color singlet, the Higgs does not couple directly to gluons. However, as no fundamental symmetry forbidding it is present [2] it can via a loop of a colored and massive particle. In the SM such states are the heavy quarks. Let us consider one quark at the time, i.e., the diagram(s) shown in Fig. 1. The first observation to make, even before starting the calculation, is that even though a triangle loop in general can give rise to divergences, both in the ultra-violet (UV) and in the infrared (IR), in this case we expect a finite result. There are several different ways of convincing that this must be the case. A simple one goes as follows. Divergent terms always factorize over lower order amplitudes. The one-loop amplitude is the first non-zero term contributing to $gg \to H$ in the perturbative expansion. Therefore there cannot be any divergence. A finite amplitude, however, does not mean that a consistent regularisation procedure is not needed. The reason is that in intermediate steps of the calculation infinities are found that cancel at the end, yet might leave finite terms. As we will see in $gg \to H$ such finite terms are actually necessary to guarantee the gauge invariance of the result, clearly showing that there is no ambiguity in the procedure. [3]

To evaluate the diagram of Fig. 1 (there are actually two diagrams, the one shown and another one with the gluons exchanged. They give the same contribution so we'll just multiply our final result by two), we employ use dimensional regularisation in $d = 4 - 2\epsilon$ dimensions. [4]

[2] In fact, classically, scale invariance would forbid such a coupling. However, scale invariance is broken by renormalisation and therefore it is not a symmetry.

[3] Less obvious is the case of $\gamma\gamma \to H$ where the contribution coming from gauge bosons loop has to be done in different gauges (or via low-energy-theorems) to prove the uniqueness and the correctness of dimensional regularisation procedure. Interestingly enough, people seem to forget this fact quite regularly over the years.

[4] Dimensional regularisation comes in several different flavors and attention has to be paid to the details of the implementation. All formulas quoted in the main body of these lecture notes are in the so-called Conventional Dimensional Regularization (CDR) which is the regularisation procedure where the $\overline{\text{MS}}$ scheme is defined. In practice, NLO calculations nowadays are done in a different scheme which limits the use of the d-dimensional Dirac algebra to the loop computation.

Using the QCD Feynman rules [QCD: Fig. 3] and the Yukawa interaction, the expression for the amplitude corresponding to the diagram of Fig. 1 reads:

$$i\mathcal{A} = -(-ig_s)^2 \mathrm{Tr}(t^a t^b)\left(\frac{-im_Q}{v}\right)\int \frac{d^d\ell}{(2\pi)^d}\frac{t^{\mu\nu}}{\mathrm{Den}}(i)^3\epsilon_\mu(p)\epsilon_\nu(q) \tag{9}$$

where the overall minus sign is due to the closed fermion loop.[5] The denominator is $\mathrm{Den} = (\ell^2 - m_Q^2)[(\ell+p)^2 - m_Q^2][(\ell-q)^2 - m_Q^2]$. Emplyoing the usual Feynman parametrization method to combine the denominators of the loop integral into one:

$$\frac{1}{ABC} = 2\int_0^1 dx \int_0^{1-x} \frac{dy}{[Ax + By + C(1-x-y)]^3} \tag{10}$$

one obtains

$$\frac{1}{\mathrm{Den}} = 2\int dx\, dy \frac{1}{[\ell^2 - m_Q^2 + 2\ell\cdot(px - qy)]^3}. \tag{11}$$

The next step is to shift the integration momenta to $\ell' = \ell + px - qy$ so the denominator takes the form

$$\frac{1}{\mathrm{Den}} \to 2\int dx\, dy \frac{1}{[\ell'^{\,2} - m_Q^2 + m_H^2 xy]^3}. \tag{12}$$

The numerator of the loop integral in the shifted loop momentum becomes

$$\begin{aligned} t^{\mu\nu} &= \mathrm{Tr}\Big[(\not\ell + m_Q)\gamma^\mu(\not\ell + \not p + m_Q)(\not\ell - \not q + m_Q)\gamma^\nu\Big] \\ &= 4m_Q\left[g^{\mu\nu}(m_Q^2 - \ell^2 - \frac{m_H^2}{2}) + 4\ell^\mu\ell^\nu + p^\nu q^\mu\right]. \end{aligned} \tag{13}$$

where we have used the fact that for transverse gluons, $\epsilon(p)\cdot p = 0$ and so terms proportional to the external momenta, p_μ or q_ν, have been dropped. The above expression shows already several interesting aspects.

The first one is that the trace is proportional to the heavy quark mass. This can be easily understood as an effect of the spin-flip coupling of the Higgs. Gluons or photons do not change the spin of the fermion, as vectors map left (right) spinors into left (right) spinors, while the scalars do couple left (right) spinors with right (left) ones. If the quark circulating in the loop is massless then the trace vanishes due to helicity conservation, independently of the actual Yukawa coupling. This is the reason why even when the Yukawa coupling of the light quark and the Higgs is enhanced (such as in SUSY or 2HDM with large $\tan\beta$), the contribution is anyway suppressed by the kinematical mass.

The second point is that simple power counting shows that the terms proportional to the squared loop momentum ℓ^2 and $\ell^\mu\ell^\nu$ give rise to UV divergences. This means that an intermediate and consinstent regularisation prescription is needed for intermediate manipulations and that divergences will have to cancel in the final result.

By shifting momenta in the numerator, dropping terms linear in ℓ' and using the relation

$$\int d^dk \frac{k^\mu k^\nu}{(k^2 - C)^m} = \frac{1}{d}g^{\mu\nu}\int d^dk \frac{k^2}{(k^2 - C)^m} \tag{14}$$

to write the amplitude in the form

$$i\mathcal{A} = -\frac{2g_s^2 m_Q^2}{v}\delta^{ab}\int\frac{d^d\ell'}{(2\pi)^d}\int dxdy\left\{g^{\mu\nu}\left[m_Q^2 + \ell'^2\left(\frac{4-d}{d}\right) + m_H^2(xy - \frac{1}{2})\right]\right.$$

[5] $\epsilon_\mu(p)$ are the transverse gluon polarizations.

$$+p^\nu q^\mu(1-4xy)\Big\}\frac{2dxdy}{(\ell'^2-m_Q^2+m_H^2xy)^3}\epsilon_\mu(p)\epsilon_\nu(q). \tag{15}$$

This expression shows that if one computes the integral in $d=4$, the UV divergent term is absent. For $d=4-2\epsilon$, however, this gives rise to a left-over finite piece, as the scalar integrals are given by

$$\begin{aligned}\int\frac{d^d\ell}{(2\pi)^d}\frac{\ell^2}{(\ell^2-C)^3} &= \frac{i}{32\pi^2}(4\pi)^\epsilon\frac{\Gamma(1+\epsilon)}{\epsilon}(2-\epsilon)C^{-\epsilon}\\ \int\frac{d^d\ell}{(2\pi)^d}\frac{1}{(\ell^2-C)^3} &= -\frac{i}{32\pi^2}(4\pi)^\epsilon\Gamma(1+\epsilon)C^{-1-\epsilon}.\end{aligned} \tag{16}$$

So it is manifest that the divergence $1/\epsilon$ cancels against the $(4-d)/d$ term leaving a finite piece, which in fact ensures that the final result is gauge invariant. By combining it with the other terms in the squared parenthesis we obtain

$$\mathcal{A}(gg\to H)=-\frac{\alpha_S m_Q^2}{\pi v}\delta^{ab}\left(g^{\mu\nu}\frac{m_H^2}{2}-p^\nu q^\mu\right)\epsilon_\mu(p)\epsilon_\nu(q)\int dxdy\left(\frac{1-4xy}{m_Q^2-m_H^2xy}\right). \tag{17}$$

(Note that we have multiplied by 2 in Eq. (17) to include the diagram where the gluon legs are crossed.) The Feynman integral of Eq. (17) can easily be performed to find an analytic result if desired. Note that the tensor structure could have been predicted from the start by imposing gauge invariance, i.e., $p^\mu\mathcal{A}^{\mu\nu}=q^\nu\mathcal{A}^{\mu\nu}=0$. By defining $I(a)$ as

$$I(a)\equiv\int_0^1 dx\int_0^{1-x}dy\frac{1-4xy}{1-axy},\qquad a=\frac{m_H^2}{m_Q^2}, \tag{18}$$

one can factorise a $1/m_Q^2$ out of the integral and cancel the overall m_Q^2 in front of the amplitude (17). In other terms the heavy quark mass dependence is confined in $I(a)$.
For a light quark, $m_Q\ll m_H$,

$$I(a)\overset{a\to\infty}{\longrightarrow}-\frac{1}{2a}\log^2 a=-\frac{m_Q^2}{2m_H^2}\log^2\frac{m_Q^2}{m_H^2}, \tag{19}$$

showing that in the Standard Model the charm and bottom quark contributions are strongly suppressed by the square of the quark mass over Higgs mass ratio and come with a minus sign (with respect to the top-quark one).
The opposite limit, $m_H\ll m_Q$,

$$I(a)\overset{a\to 0}{\longrightarrow}\frac{1}{3}, \tag{20}$$

which is found to be an extremely good approximation even for $m_Q\sim m_H$, is quite surprising at first. In this case the amplitude reads

$$\mathcal{A}(gg\to H)\overset{m_Q\gg m_H}{\longrightarrow}-\frac{\alpha_S}{3\pi v}\delta^{ab}\left(g^{\mu\nu}\frac{m_H^2}{2}-p^\nu q^\mu\right)\epsilon_\mu(p)\epsilon_\nu(q). \tag{21}$$

i.e., the amplitude $gg\to H$ becomes *independent* of the mass of the heavy fermion in the loop. This is a special case of a general low energy theorem (which holds in the $p_H\to 0$ limit) that states that if the colored particle mass, independently of the other quantum numbers such as its spin acquires (all of) its mass via the Higgs mechanism, it will contribute to the amplitude $gg\to H$ independently of its mass. In other words $gg\to H$ acts as a counter of heavy colored particles. In a four generation scenario, for instance, the contribution from the t' and b' would lead to a factor of three increase at the amplitude level, i.e. a factor 9 at the cross section level. Note that this is in an apparent contradiction with of our intuition

that heavy particles should decouple and not affect the physics at lower energy. The heavy states would not decouple because of our assumption that their (whole) mass is due to electroweak symmetry breaking and the interaction with the Higgs. Another interesting case is that of SUSY, where down-type and up-type quarks can couple differently to the Higgs(es) and other colored states (squarks) are present in the spectrum. At large $\tan\beta$, i.e. when $m_b \tan\beta \simeq m_t$, the Higgs bottom couplings are enhanced by a factor $\tan\beta$, while those of the top suppressed by a $\cot\beta$. However, the scaling with masses is different in the two limits and the contribution from the bottom anyway suppressed by m_Q/m_H. In addition, the the two contributions will have an opposite sign so that will actually interfere destructively in the amplitude squared. What about the squark contributions? Being heavy scalars and therefore coming with an opposite sign shouldn't the stop cancel exactly the contributions from the top and the others squarks give the dominant contribution? In this case, one has to remember that in (possibly) realistic SUSY models the mass of a squark has two sources: one from the coupling to the Higgs vev, which due to SUSY, it is exactly equal to the SM partner coupling and the other from the SUSY soft-breaking terms. For light quarks the latter are by far dominant giving a scaling for $\mathcal{A}$ of the type $m_q/m_{\tilde{q}}$, so highly suppressed and decoupling. A light stop instead, $m_{\tilde{t}} \simeq m_t$ could lead to a possibly strong suppression of $\mathcal{A}$.

3.2 Total cross section at the LHC at LO

The result can be written as:

$$\sigma^{\rm LO}(pp \to H + X) = \frac{\alpha_S^2(\mu_R)}{64\pi v^2} \mid I\left(\frac{m_H^2}{m_Q^2}\right) \mid^2 \tau_0 \int_{\log\sqrt{\tau_0}}^{-\log\sqrt{\tau_0}} dy g(\sqrt{\tau_0}e^y, \mu_F) g(\sqrt{\tau_0}e^{-y}, \mu_F) \qquad (22)$$

Using LO PDF's available in public libraries, such as LHAPDF [17] one can easily compute the gluon-gluon luminosity and therefore the LO Higgs cross section at the LHC14, see Fig. 2. An example is given in a Mathematica® notebook that can be found at the web address mentioned at the end of the Introduction. An interesting exercise is to vary the value of the renormalisation and factorisation scales around the natural central choice $\mu_R = \mu_F = m_H$ to try to estimate the unknown higher-orders terms in the perturbative expansion. It has to be noted that at LO, the cross section depends on μ_R only through $\alpha_S(\mu_R)$ which appears in the short distance coefficient and therefore as an overall factor α_S^2, and depends on μ_F only via the PDF's (both dependences are of logarithmic nature, as the application of the renormalisation group equations easily shows). In other words the dependence on the scales is maximal as there is no explicit dependence on the $\log$ of the scales in the short distance coefficients that can compensate those in the coupling and in the PDF's. At this order, this is consistent as scale changes correspond to a change of at least one order in α_S more and in a LO computation only the first term in the perturbative expansion is present. The result of varying the scales independently $1/2 m_H < \mu_R, \mu_F < 2m_H$ with $1/2 < \mu_F/\mu_R < 2$ in the LO predictions for the LHC is shown in Fig. 9 for different Higgs masses. Result are normalized to the central reference choice $\mu_R = \mu_F = m_H$.

4 Higgs Effective field theory

The main result of the simple calculation $gg \to H$ is that gluon fusion is basically independent of the heavy quark mass for a light Higgs boson. The result of Eq. (33) can be easily derived starting from the effective vertex,

$$\begin{aligned} \mathcal{L}_{\rm eff} &= \frac{\alpha_S}{12\pi} G^a_{\mu\nu} G^{a\,\mu\nu} \left(\frac{H}{v}\right) \\ &= \frac{\beta_F}{g_s} G^a_{\mu\nu} G^{a\,\mu\nu} \left(\frac{H}{2v}\right)(1-\delta), \end{aligned}$$

where

$$\beta_F = \frac{g_s^3 N_F}{24\pi^2} \qquad (23)$$

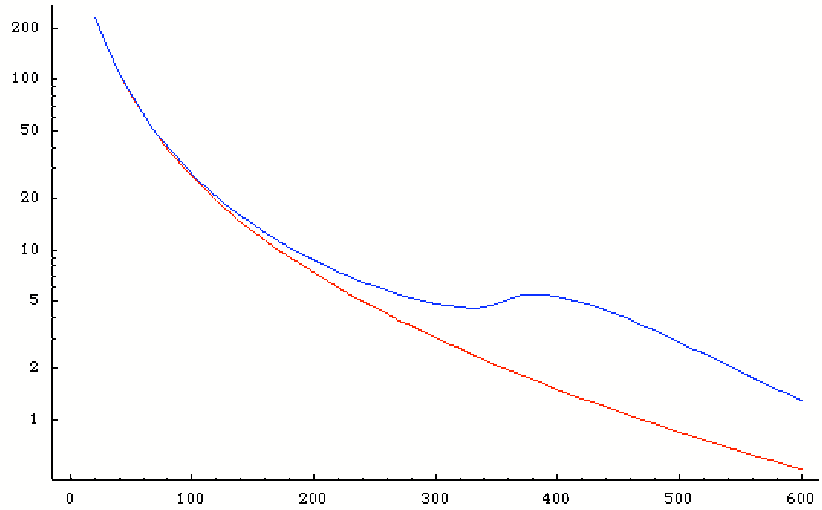

Figure 2: Example of a plot for the LO cross section for $pp \to H$ at the LHC14 (pb) as a function of the Higgs mass (GeV) obtained with Mathematica® notebook available from the author (link in the text). The red (lower) curve is the large top-mass limit, while the blue (upper) curve is the result withe the full top-mass dependence.

is the contribution of heavy fermion loops to the $SU(3)$ beta function and $\delta = 2\alpha_S/\pi$.[6] (N_F is the number of heavy fermions with $m \gg m_H$.) The effective Lagrangian of Eq. (23) gives ggH, $gggH$ and $ggggH$ vertices and can be used to compute the radiative corrections of $\mathcal{O}(\alpha_S^3)$ to gluon production. The correction in principle involve 2-loop diagrams. However, using the effective vertices from Eq. (23), the $\mathcal{O}(\alpha_S^3)$ corrections can be found from a 1-loop calculation. To fix the notation we shall use

$$\mathcal{L}_{\text{eff}} = -\frac{1}{4} A H G^a_{\mu\nu} G^{a,\mu\nu}, \tag{24}$$

where $G^a_{\mu\nu}$ is the field strength of the SU(3) color gluon field and H is the Higgs-boson field. The effective coupling A is given by

$$A = \frac{\alpha_S}{3\pi v}\left(1 + \frac{11}{4}\frac{\alpha_S}{\pi}\right), \tag{25}$$

where v is the vacuum expectation value parameter, $v^2 = (G_F\sqrt{2})^{-1} = (246)^2$ GeV^2 and the α_S correction is included, as discussed above. The effective Lagrangian generates vertices involving the Higgs boson and two, three or four gluons. The associated Feynman rules are displayed in Fig. 3. The two-gluon–Higgs-boson vertex is proportional to the tensor

$$H^{\mu\nu}(p_1, p_2) = g^{\mu\nu} p_1 \cdot p_2 - p_1^\nu p_2^\mu, \tag{26}$$

while the vertices involving three and four gluons and the Higgs boson are exactly proportional to their counterparts from pure QCD

$$V^{\mu\nu\rho}(p_1, p_2, p_3) = (p_1 - p_2)^\rho g^{\mu\nu} + (p_2 - p_3)^\mu g^{\nu\rho} + (p_3 - p_1)^\nu g^{\rho\mu}, \tag{27}$$

and

$$X^{\mu\nu\rho\sigma}_{abcd} \quad = \quad f_{abe} f_{cde}(g^{\mu\rho} g^{\nu\sigma} - g^{\mu\sigma} g^{\nu\rho}) + f_{ace} f_{bde}(g^{\mu\nu} g^{\rho\sigma} - g^{\mu\sigma} g^{\nu\rho})$$

[6] The $(1-\delta)$ term arises from a subtlety in the use of the low energy theorem. Since the Higgs coupling to the heavy fermions is $M_f(1 + \frac{H}{v})\overline{f}f$, the counterterm for the Higgs Yukawa coupling is fixed in terms of the renormalisation of the fermion mass and wavefunction. The beta function, on the other hand, is evaluated at $q^2 = 0$. The $1 - \delta$ term corrects for this mismatch.

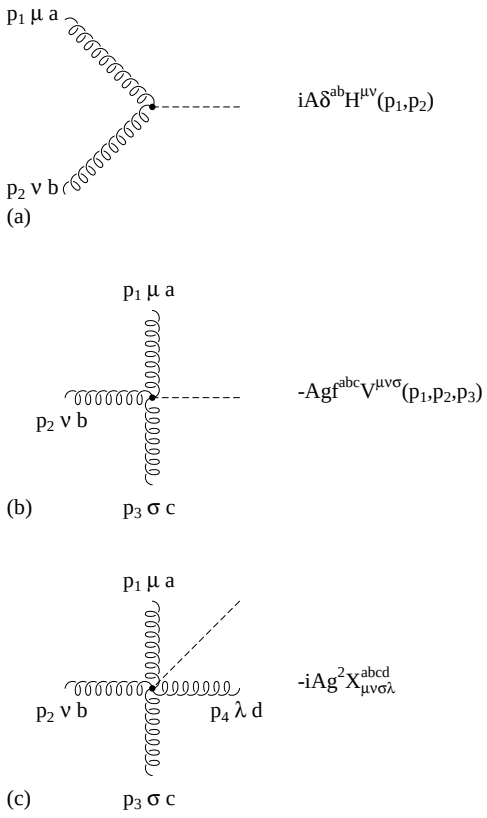

Figure 3: Feynman rules in the EFT where the top quark is integrated out. Gluon momenta are outgoing.

$$+ \quad f_{ade}f_{bce}(g^{\mu\nu}g^{\rho\sigma} - g^{\mu\rho}g^{\nu\sigma}). \tag{28}$$

5 $gg \to$ Higgs @ NLO

The HEFT is clearly a very powerful approximation as it turns a loop computation into a tree-level one. That means that within the HEFT the calculation of the total cross section for Higgs production at NLO will appear as a usual NLO calculation, i.e., involving only one-loop and tree-level diagrams. This is what we describe in this section.

5.1 The NLO computation in a nutshell

At NLO Eq. 3 can be rewritten as

$$\begin{aligned}\sigma^{\rm NLO}(H+X) &= \int_{\tau_0}^1 dx_1 \int_{\tau_0/x_1}^1 dx_2 f_g(x_1,\mu_F) f_g(x_2,\mu_F)[\hat{\sigma}_B^{(0)}(gg\to H) + \hat{\sigma}_V^{(1)}(gg\to H)] \\ &+ \sum_{ijk}\int_{\tau_0}^1 dx_1 \int_{\tau_0/x_1}^1 dx_2 f_i(x_1,\mu_F) f_j(x_2,\mu_F) \times \hat{\sigma}_R^{(1)}(ij\to H\,k)\,, \end{aligned} \tag{29}$$

where $\hat{\sigma}^{(0)}(gg \to H)$ and $\hat{\sigma}_V^{(1)}(gg \to H)$ denote the Born-level and the virtual cross sections, while $\hat{\sigma}_R^{(1)}(ij \to H\,k)$ is the real-emission cross section:

$$\hat{\sigma}_{B,V}^{(0,1)}(gg\to H) = \frac{1}{2s}\overline{|\mathcal{A}_{B,V}|}^2 d\Phi_B\,,$$

$$\hat{\sigma}_R^{(1)}(ij \to Hk) \;=\; \frac{1}{2s}\overline{|\mathcal{A}_R|}^2 d\Phi_R\,,$$

In general, the virtual term contains ultraviolet (UV), soft and collinear divergences. The UV divergences are absorbed by a universal redefinition of the couplings entering at the Born amplitude, as dictated by the renormalisation of the SM. When integrated over the full real phase space, the real term generates soft and collinear divergences, too, and only when *infrared(IR)-safe* quantities are computed, these divergences cancel to yield a finite result. IR-safe observables $O(\Phi)$ can be best understood by considering the soft or collinear limit in the real phase space, i.e. when the additional parton has low energy or is parallel to another parton. In this limit, an IR-safe observable yields $\lim O(\Phi_R) = O(\Phi_B)$, where the Born-level configuration Φ_B is obtained from Φ_R by eliminating the soft particle (in case of soft singularities) or by merging the collinear particles (in case of collinear singularities).

There several ways to handle the cancellation of the singularities, which fall into two large categories, process-dependent and process-independent methods. In the former, one treats each calculation/process independently and performs manipulations of the integrals over the phase space so to obtain analytic or semi-analytic results.

Process independent methods, on the other hand, are based on a very fundamental result, i.e., that the pattern of the soft and collinear divergences is universal and depends only on the quantum numbers of the initial and final state particles in the Born process. That means that given the Born amplitude, one can predict the divergences that will show up in the virtual contributions and will be then cancelled over integration of the extra radiation in the reals. More importantly, such divergences come in just a handful of different types that can be dealt with once and for all.

Let us now rewrite Eq. (30) in a general and short-hand notation

$$\sigma^{\rm NLO} \;\equiv\; \int \mathrm{d}\Phi_B \left[B(\Phi_B) + V(\Phi_B)\right] O(\Phi_B) + \int \mathrm{d}\Phi_R R(\Phi_R)\, O(\Phi_R) \tag{30}$$

which will be useful in the following. A NLO cross section is written in terms of matrix elements for the Born and virtual integrated over the Born phase space plus the real matrix elements integrated over the real phase space. Within a subtraction method, the real phase space is parametrized in terms of an underlying Born phase space Φ_B and a radiation phase space $\Phi_{R|B}$. A necessary requirement upon this parametrization is that, in the singular limits, by merging collinear partons, or eliminating the soft parton, the real phase becomes equal to the underlying Born one. Then the expectation value of an IR-safe observable reads

$$\begin{aligned}\int \mathrm{d}\sigma^{(\rm NLO)} O(\Phi) \;&=\; \int \mathrm{d}\Phi_B \left[B(\Phi_B) + V(\Phi_B) + \int \mathrm{d}\Phi_{R|B} S(\Phi_R)\right] O(\Phi_B) \\ &+\; \int \mathrm{d}\Phi_R \left[R(\Phi_R)\, O(\Phi_R) - S(\Phi_R) O(\Phi_B)\right]\,. \end{aligned} \tag{31}$$

The third member of the above equation is obtained by adding and subtracting the same quantity from the two terms of the second member. The terms $S(\Phi_{R|B})$ are the subtraction terms, which contain all soft and collinear singularities of the real-emission term. Using the universality of soft and collinear divergences, they are written in a factorised form as

$$S(\Phi_R) = B(\Phi_B) \otimes \tilde{S}(\Phi_{R|B})\,, \tag{32}$$

where the $\tilde{S}(\Phi_{R|B})$ can be composed from universal, process-independent subtraction kernels with analytically known (divergent) integrals. These integral, when summed and added to the virtual term, yield a finite result. The second term of the last member of Eq. (31) is also finite if O is an IR-safe observable, since by construction S cancels all singularities in R in the soft and collinear regions. The most popular subtraction schemes currently used in public NLO codes are based on the dipole subtraction [18] and the

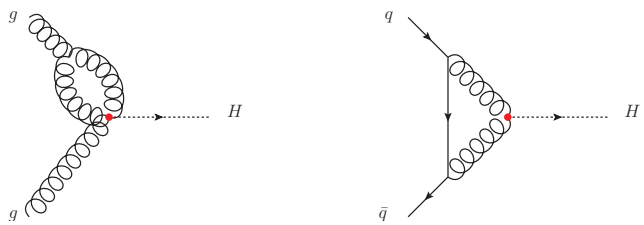

Figure 4: Example of Feynman diagrams giving null contributions to $ij \to H$ at one-loop in the HEFT. Bubbles on the gluon legs are zero in dimensional regularisation. $q\bar{q} \to H$ is zero at all orders in perturbation theory if $m_q = 0$ due to chiral symmetry.

so-called FKS scheme [19]. The case of $gg \to H$ at NLO is particularly simple as the Born amplitude is a $2 \to 1$ process. This means that the integration over phase space of the real corrections is particularly simple and can therefore be done analytically. This has also the pedagogical advantage that shows explicitly where the divergences come from and to "see" the cancellations term by term. We study the process $gg \to H$ at NLO, in the large top-quark mass limit. All results given below are in Conventional Dimensional Regularization (CDR), where matrix elements are calculated in d dimensions, including the Born and real contributions, as well as the integration over phase space [6].

5.2 $gg \to H$: Born in d dimensions

The Born amplitude is calculated via the HEFT feynman rules. The only difference with respect to the previous calculation stems from the fact that now the computation has to be done in $d = 4 - 2\epsilon$-dimensions, with ϵ infinitesimal. The phase space do not bring any extra ϵ term. However, the matrix element changes

$$\left(g^{\mu\nu}\frac{m_H^2}{2} - p^\nu q^\mu\right)^2 = \frac{1}{4}(d-2)m_H^4\,, \tag{33}$$

as well as the average over the initial state gluon polarizations which in d-dimensions are $d-2$. This gives

$$\begin{aligned}\hat{\sigma}_B &= \frac{\alpha_S^2}{\pi}\frac{m_H^2}{576v^2 s}\frac{\mu^{2\epsilon}}{(1-\epsilon)}\,\delta(1-z) \\ &\equiv \hat{\sigma}_0\,\delta(1-z)\,,\end{aligned} \tag{34}$$

where $z \equiv m_H^2/s$ is the inelasticity of the process, i.e. the fraction of the parton parton energy that goes into the Higgs (for the Born $z = 1$). μ is the usual arbitrary scale that needs to be introduced in dimensional regularisation to correct for the different dimensions and keep the action adimensional ($\hbar = c = 1$). Note that a cross section in d dimensions has dimensions $[\sigma] = M^{2-d}$. Also note that we have defined $\hat{\sigma}_0$ as containing an explicit factor z.

5.3 $gg \to H$: virtual corrections

There are several diagrams appearing at one-loop. Diagrams involving bubbles on the external gluon legs (with 3-point gluon-gluon-gluon and gluon-gluon-Higgs verteces) give rise to scaleless integrals that are zero in dimensional regularisation, see Fig. 4, left diagram. The $q\bar{q} \to H$ process, see Fig 4 right, is

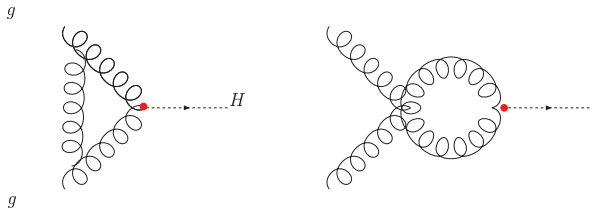

Figure 5: Feynman diagrams giving non-zero contributionsto $gg \to H$ at one-loop in the HEFT.

proportional to the m_q parton mass which are taken massless and therefore null at all orders. As a result, only two diagrams are non-zero, i.e., the vertex correction and the bubble with the four gluon vertex as shown in Fig. 5

$$\hat{\sigma}_{\rm tri} = \hat{\sigma}_0\, \delta(1-z)\, \left[1 + \frac{\alpha_S}{2\pi} C_A \left(\frac{\mu^2}{m_H^2}\right)^{\epsilon} c_\Gamma \left(-\frac{2}{\epsilon^2} + \frac{10}{3\epsilon} + \frac{179}{36} + \pi^2\right)\right], \tag{35}$$

$$\hat{\sigma}_{\rm bub} = \hat{\sigma}_0\, \delta(1-z)\, \left[1 + \frac{\alpha_S}{2\pi} C_A \left(\frac{\mu^2}{m_H^2}\right)^{\epsilon} c_\Gamma \left(-\frac{10}{3\epsilon} - \frac{179}{36}\right)\right], \tag{36}$$

where

$$c_\Gamma = (4\pi)^\epsilon \frac{\Gamma(1+\epsilon)\Gamma(1-\epsilon)^2}{\Gamma(1-2\epsilon)}\,. \tag{37}$$

To obtain the results above, one has to write down the loop amplitudes, perform a few simplifications and the decomposition of the tensor integrals appearing in the amplitudes so to express the results in terms of the following two scalar integrals:

$$\begin{aligned}
\mu^{2\epsilon} \int \frac{{\rm d}^d\ell}{(2\pi)^d} \frac{1}{\ell^2(\ell+p_H)^2} &= c_\Gamma \left(\frac{\mu^2}{m_H^2}\right)^{\epsilon} \left(\frac{1}{\epsilon} + 2\right), \\
\mu^{2\epsilon} \int \frac{{\rm d}^d\ell}{(2\pi)^d} \frac{1}{\ell^2(\ell+p_1)^2(\ell+p_2)^2} &= \frac{c_\Gamma}{2m_H^2} \left(\frac{\mu^2}{m_H^2}\right)^{\epsilon} \left(\frac{2}{\epsilon^2} - \pi^2\right),
\end{aligned} \tag{38}$$

with $p_H = p_1 + p_2$. Summing the contributions of the two diagrams above with the α_S correction from Eq. (25), we obtain

$$\hat{\sigma}_V = \hat{\sigma}_0\, \delta(1-z)\, \left[1 + \frac{\alpha_S}{2\pi} C_A \left(\frac{\mu^2}{m_H^2}\right)^{\epsilon} c_\Gamma \left(-\frac{2}{\epsilon^2} + \frac{11}{3} + \pi^2\right)\right], \tag{39}$$

i.e., the total virtual contribution is proportional to the Born amplitude and it contains pole(s) in powers of $1/\epsilon$. The fact that the full virtual amplitude is proportional to the Born is due to the simplicity of a $2 \to 1$ process. However, in general one can prove that the divergent contributions must be proportional to the Born in the case of collinear (and collinear-soft, the double pole) divergences and to the so-called color-connected Born for the soft ones. Given that the Born amplitude is proportional to α_S^2 and we are calculating QCD corrections, we also expect UV divergences, which are proportional to $1/\epsilon$. The fact that apparently we do not see any pole in $1/\epsilon$ in the result above, it simply means that there is an accidental cancellation between simple poles of IR origin and that of UV origin, as we did not keep them distinct in the calculation. To leave only IR poles in the amplitude to be cancelled with those coming from the real contribution, we therefore proceed here to renormalisation of α_S. This can be attained by the substitution in $\hat{\sigma}_0$, see also [QCD:1.2.3],

$$\alpha_S \to \alpha_S^{\overline{\rm MS}}(\mu_R) = \alpha_S \left[1 - \frac{\alpha_S}{2\pi} c_\Gamma \left(\frac{\mu^2}{\mu_R^2}\right)^{\epsilon} \frac{b_0}{\epsilon}\right], \tag{40}$$

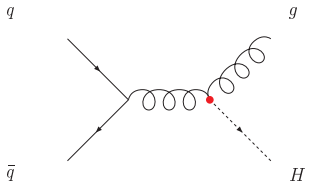

Figure 6: Feynman diagrams giving $q\bar{q}$ real contributions in the infinite top-quark mass limit. These contributions are finite.

where $b_0 = 11/6\, C_A - 2n_f T_F/3$. The UV-renormalized virtual amplitude is

$$\hat{\sigma}_V^{\overline{\rm MS}}(gg) = \hat{\sigma}_0\ \delta(1-z)\ \left[1 + \frac{\alpha_S}{2\pi} C_A \left(\frac{\mu^2}{m_H^2}\right)^{\epsilon}\ c_\Gamma \left(-\frac{2}{\epsilon^2} - \frac{2}{\epsilon}\frac{b_0}{C_A} - 2\frac{b_0}{C_A}\log\frac{m_H^2}{\mu_R^2} + \frac{11}{3} + \pi^2\right)\right] . \quad (41)$$

where now the poles in $1/\epsilon^2$, $1/\epsilon$ are only of IR nature. Another important feature which is manifest in the expression above is the appearance of an explicit $\log$ of the renormalisation scale in the short distance part. As mentioned before, this the improvement expected on the scale dependence of a NLO result: the μ_R dependence of the $\alpha_S^2(\mu_R)$ overall coefficient is exactly cancelled by the explicit log up to order α_S^3.

5.4 Real Contributions

Real corrections imply the calculation of $2 \to 2$ tree-level amplitudes and their integration over phase space in d dimensions. All possible initial and final state partons, gluons, quarks and anti-quarks need to be included,

1. $q\bar{q} \to Hg$ + crossing (i.e., $\bar{q}q \to Hg$),
2. $qg \to Hq$ + crossings (i.e., $\bar{q}g \to H\bar{q}$, $gq \to Hq$, $g\bar{q} \to H\bar{q}$),
3. $gg \to Hg$.

It is easy to predict which divergences to expect from each of the subprocesses above. The reason is that out of the possible (by Lorentz and color invariance) underlying Born amplitudes, i.e., $q\bar{q} \to H$ and $gg \to H$, the only non-zero one is $gg \to H$. Therefore the first processes must give a finite result when integrated over phase space, the second ones can only contain collinear divergences to be absorbed in quark PDF's, while the last is expected to give rise to soft and collinear divergences, part of which will be absorbed in the gluon PDF's and the rest canceled against those coming from the virtual contributions, Eq. (41).

5.4.1 $q\bar{q} \to Hg$

This contribution, shown in Fig. 6 is finite and can be calculated directly in four dimensions. A simple calculation gives

$$\overline{|\mathcal{M}|^2} = \frac{4}{81}\frac{\alpha_S^3}{\pi v^2}\ \frac{(u^2+t^2)}{s}\,, \quad (42)$$

to be integrated over the 4-dimensional phase space

$$d\Phi_2 = \frac{1}{8\pi}(1-z)\ dv\,, \quad (43)$$

where $v = 1/2(1+\cos\theta)$ and $z = m_H^2/s$ as usual. Using

$$t \;=\; -s(1-z)(1-v)\,, \quad (44)$$

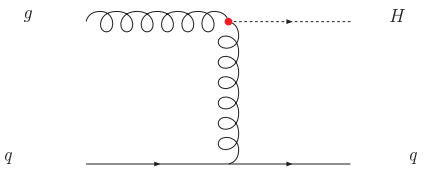

Figure 7: Feynman diagrams giving qg real contributions in the infinite top-quark mass limit.

$$u = -s(1-z)v\,, \tag{45}$$

gives

$$\hat{\sigma}_R(q\bar{q}) = \hat{\sigma}_0 \frac{\alpha_S}{2\pi}\frac{64}{27}\frac{(1-z)^3}{z}\,. \tag{46}$$

5.4.2 $gq \to Hq$

Let us consider now the contribution from the diagrams with an initial quark, i.e., the process $gq \to Hq$. The d-dimensional averaged/summed over initial/final state polarizations and colors amplitude is

$$\overline{|\mathcal{M}|^2} = -\frac{1}{54(1-\epsilon)}\frac{\alpha_S^3}{\pi v^2}\,\frac{(u^2+s^2)-\epsilon(u+s)^2}{t}\,. \tag{47}$$

Integrating it over the d-dimensional phase space

$$d\Phi_2 = \frac{1}{8\pi}\left(\frac{4\pi}{s}\right)^{\epsilon}\frac{1}{\Gamma(1-\epsilon)}\,z^{\epsilon}(1-z)^{1-2\epsilon}\,v^{-\epsilon}(1-v)^{-\epsilon}dv \tag{48}$$

one gets

$$\hat{\sigma}_R(gq) = \hat{\sigma}_0\,\frac{\alpha_S}{2\pi}C_F\left(\frac{\mu^2}{m_H^2}\right)^{\epsilon}\,c_\Gamma\,\left[-\frac{1}{\epsilon}p_{gq}(z) + z - \frac{3}{2}\frac{(1-z)^2}{z} + p_{gq}(z)\log\frac{(1-z)^2}{z}\right], \tag{49}$$

where the $p_{gq}(z)$ color-stripped Altarelli-Parisi splitting function is given in the Appendix, Eqs. (67). We perform the factorisation of the collinear divergences adding the counterterm

$$\sigma^{\rm coll.}_{\rm c.t.}(gq) = \sigma_0\frac{\alpha_S}{2\pi}\,\left[\left(\frac{\mu^2}{\mu_F^2}\right)^{\epsilon}\frac{c_\Gamma}{\epsilon}P_{gq}(z)\right]. \tag{50}$$

We note that in fact in CDR the cross section factorises over the d-dimensional splitting functions Eqs. (68). However, the collinear counter-term in $\overline{\rm MS}$ is defined with the 4-dimensional Altarelli-Parisi splitting functions, Eqs. (67), and that is why we have written the result above in terms of $p_{gq}(z)$ leaving out a finite term z (also note that our definition of σ_0, Eq. (34), contains a factor z). This gives

$$\begin{aligned}\hat{\sigma}_R^{\overline{\rm MS}}(gq) &= \hat{\sigma}_R(gq) + \hat{\sigma}^{\rm coll.}_{\rm c.t.}(gq)\\ &= \sigma_0\,\frac{\alpha_S}{2\pi}C_F\,\left[p_{gq}(z)\log\frac{m_H^2}{\mu_F^2} + p_{gq}(z)\log\frac{(1-z)^2}{z} + z - \frac{3}{2}\frac{(1-z)^2}{z}\right].\end{aligned} \tag{51}$$

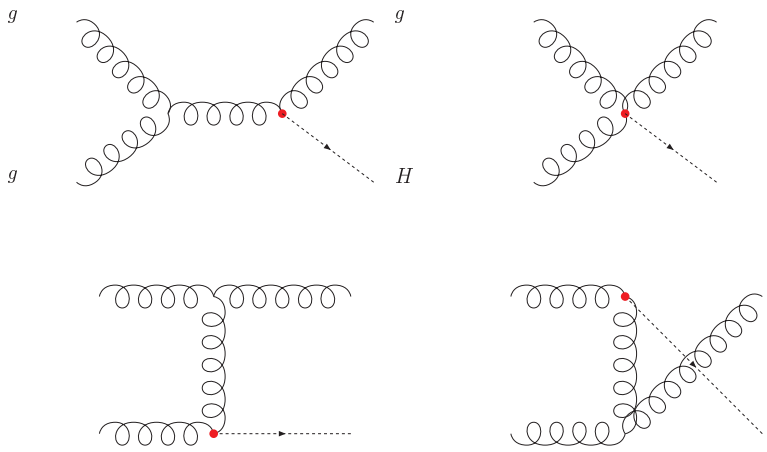

Figure 8: Feynman diagrams giving gg real contributions in the infinite top-quark mass limit.

5.4.3 $gg \to Hg$

The calculation of the d-dimensional $gg \to Hg$ amplitude involves the four diagrams shown in Fig. 8 and it is not so trivial to do by hand, yet the final result is very compact:

$$\overline{|\mathcal{M}|^2} = \frac{1}{24(1-\epsilon)^2}\frac{\alpha_S^3}{\pi v^2}\frac{(m_H^8+s^4+t^4+u^4)(1-2\epsilon)+\frac{1}{2}\epsilon(m_H^4+s^2+t^2+u^2)^2}{stu}\,. \tag{52}$$

This example is illustrative of the fact that keeping track of the ϵ parts in the amplitude squared makes the calculation significantly more complex for at least two reasons. First the structure of the result itself is more involved. Second, one is forced to work at the squared amplitude level as d dimensional contributions come from the ($d-2$ dimensional) gluon polarizations and therefore cannot exploit the beauty, power and simplicity of helicity amplitude techniques [20, 21]. Computing QCD amplitudes where states have fixed polarizations entails huge simplifications and allows to make predictions for amplitudes with many external partons. For example, tree-level amplitudes in the HEFT involving up to 5 extra partons can be easily obtained automatically using tools such as ALPGEN [22] or MADGRAPH [23]. Fortunately, it turns out that is possible to use a different scheme than CDR and actually perform the computation of the Born and real matrix elements in exactly four dimensions (yet integrate them over the d-dimensional phase space). This involves a different (and a bit tricky) d-dimensional algebra for the loop computations and the introduction of (universal) finite terms for the initial-state counter-terms and UV subtractions, yet with an enormous computational simplification. All public NLO codes for processes at the LHC in practice do use such "maximally four dimensional" d-dimensional regularisation schemes. Integrating the amplitude (52) over the d-dimensional phase space of Eq. (48) gives

$$\begin{aligned}\hat{\sigma}_R(gg) \;=\; & \hat{\sigma}_0\,\frac{\alpha_S}{2\pi}C_A\left(\frac{\mu^2}{m_H^2}\right)^{\epsilon} c_\Gamma\left[\left(\frac{2}{\epsilon^2}+\frac{2}{\epsilon}\frac{b_0}{C_A}-\frac{\pi^2}{3}\right)\delta(1-z)\right.\\ & -\frac{2}{\epsilon}p_{gg}(z)-\frac{11}{3}\frac{(1-z)^3}{z}-4\frac{(1-z)^2(1+z^2)+z^2}{z(1-z)}\log z\\ & \left.+\,4\frac{1+z^4+(1-z)^4}{z}\left(\frac{\log(1-z)}{1-z}\right)_+\right]\,,\end{aligned} \tag{53}$$

where the plus prescription is defined as follows:

$$\int_0^1 dx\,[h(x)]_+ f(x) = \int_0^1 dx\,h(x)[f(x) - f(1)]\,. \tag{54}$$

Note that the $\frac{2}{\epsilon}\frac{b_0}{C_A}\delta(1-z)$ in Eq. (53) comes from rexpressing the divergent term $-\frac{4}{\epsilon}[\frac{z}{(1-z)_+} + \frac{1-z}{z} + z(1-z)]$ in terms of $-\frac{2}{\epsilon}p_{gg}(z)$, see Eq. (67). The factorisation of the collinear divergence is handled by adding the corresponding counterterm

$$\hat{\sigma}^{\rm coll.}_{\rm c.t.}(gg) = 2\,\hat{\sigma}_0 \frac{\alpha_S}{2\pi}\,\left[\left(\frac{\mu^2}{\mu_F^2}\right)^{\epsilon} \frac{c_\Gamma}{\epsilon} P_{gg}(z)\right]\,, \tag{55}$$

which gives

$$\begin{aligned}
\hat{\sigma}_R^{\overline{\rm MS}}(gg) &= \hat{\sigma}_R(gg) + \hat{\sigma}^{\rm coll.}_{\rm c.t.}(gg) \\
&= \hat{\sigma}_0\,\frac{\alpha_S}{2\pi} C_A \left(\frac{\mu^2}{m_H^2}\right)^{\epsilon} c_\Gamma\,\left[\left(\frac{2}{\epsilon^2} + \frac{2}{\epsilon}\frac{b_0}{C_A} - \frac{\pi^2}{3}\right)\delta(1-z)\right. \\
&\quad + 2p_{gg}\log\frac{m_H^2}{\mu_F^2} - \frac{11}{3}\frac{(1-z)^3}{z} - 4\frac{(1-z)^2(1+z^2)+z^2}{z(1-z)}\log z \\
&\quad \left. + 4\frac{1+z^4+(1-z)^4}{z}\left(\frac{\log(1-z)}{1-z}\right)_+\right]\,.
\end{aligned} \tag{56}$$

We can now recognise that the IR poles match those of the virtual contributions in Eq. (41). Adding up the contributions from real and virtual contributions of the gg channel we obtain (note that our definition of σ_0, Eq. (34), contains a factor z):

$$\begin{aligned}
\hat{\sigma}^{\overline{\rm MS}}(gg) &= \hat{\sigma}_R^{\overline{\rm MS}}(gg) + \hat{\sigma}_V^{\overline{\rm MS}}(gg) \\
&= \sigma_0\,\frac{\alpha_S}{2\pi} C_A \left[\left(\frac{11}{3} + \frac{2}{3}\pi^2 - 2\frac{b_0}{C_A}\log\frac{m_H^2}{\mu_R^2}\right)\delta(1-z)\right. \\
&\quad - \frac{11}{3}\frac{(1-z)^3}{z} + 2p_{gg}\log\frac{m_H^2}{\mu_F^2} - 4\frac{(1-z+z^2)^2}{z(1-z)}\log z \\
&\quad \left. + 8\frac{(1-z+z^2)^2}{z}\left(\frac{\log(1-z)}{1-z}\right)_+\right]\,.
\end{aligned} \tag{57}$$

As predicted, the final results for the short distance coefficients is finite (yet scheme dependent) and does contain the necessary $\log$'s of the renormalisation and factorisation scales that compensate up to α_S^3 the corresponding dependences in $\alpha_S^2(\mu_R)$ of the Born amplitude and in the PDF's.

5.5 NLO results: discussion

The expressions above can be easily implemented in a numerical code to perform the convolution integrals with PDF's. A few simple numerical optimizations, such as the choice of integration variables, and a bit of attention to the implementation of the + distributions, that's all is needed. The reader can find a sample implementation in a Mathematica® notebook at the web address mentioned at the end of the Introduction. By running the code with different scale choices, one can associate an uncertainty to the NLO predictions as done at LO. The result, shown in Fig. 9, comes as a big surprise! The NLO calculation predicts a rate twice as large and the respective LO and NLO uncertainty bands do not even overlap. That means that our naive estimate of the uncertainties at LO is totally off and therefore unreliable. It seems also to suggest that perturbation expansion is at stake here. As we had mentioned, this motivated the computation of the NNLO corrections, which are also shown in Fig. 9. Fortunately, NNLO

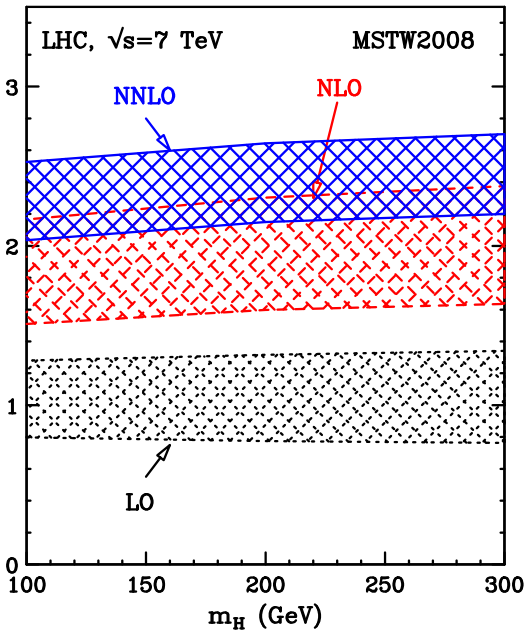

Figure 9: K-factors for Higgs production from gluon fusion at the LHC. Uncertainty bands are obtained via independent scale variation $1/2\, m_H < \mu_R, \mu_F < 2\, m_H$ with $1/2 < \mu_F/\mu_R < 2$. The LO and NLO bands can be obtained by implementing the formulas obtained in these notes in a code that perfoms the numerical integration over the PDF's. Cross-checks and NNLO results can be obtained with HNNLO [24]. (Plot courtesy of M. Grazzini).

predictions do overlap with NLO and also display a smaller scale dependence, so that the perturbation picture seems safe starting from NLO on. In fact, this behavior is rather special to $pp \to H + X$ and it is often rephrased by saying that what we call LO (in the perturbative expansion) is not actually the leading one in size and therefore we should not start from that. For instance, in Drell-Yan or VBF this does not happen, and the perturbative expansions (seem to) converge beautifully, see Fig. 10. In any case, the Higgs production reminds us an important fact that we should always keep in mind: scale variation cannot by definition reproduce missing finite terms in the perturbative expansion and as such can only give an indication of what the real uncertainties could be. On the other hand, comparison between predictions from LO and NNLO, their stabilization (or lack thereof) and the use of approximate methods to determine (classes of) higher order terms, all together can provide a rather solid picture on the theoretical uncertainties on a case-by-case basis. We mention, in passing, another important source of uncertainties in making predictions for hadron colliders, i.e., that coming from imperfect knowledge of the PDF's. Uncertainties are related to unknown higher-order terms in the DGLAP evolution equations that determine as well as from the extraction of the initial condition from experimental data, see [QCD:3] and in particular [QCD:3.3.2]. [7]

As far as total cross sections are concerned, the situation is therefore pretty clear. Fixed-order calculations come equipped with self-detecting procedures that can give us information on whether a prediction is reliable or not. If not, it can be systematically improved by including higher-order terms (almost for free nowadays at NLO, yet at a rather high cost at NNLO) and uncertainties can be easily estimated. So it is natural to ask, what about other IR-safe observables?

Let us consider, once again $pp \to H + X$ as an example, and focus on the Higgs momentum

[7] The latter does in fact imply also the prediction of experimental observables at the same order in perturbation theory and therefore are also intrinsically also affected by scale dependencies. Such effects are not included normally in the estimation of the uncertainties coming from PDF's.

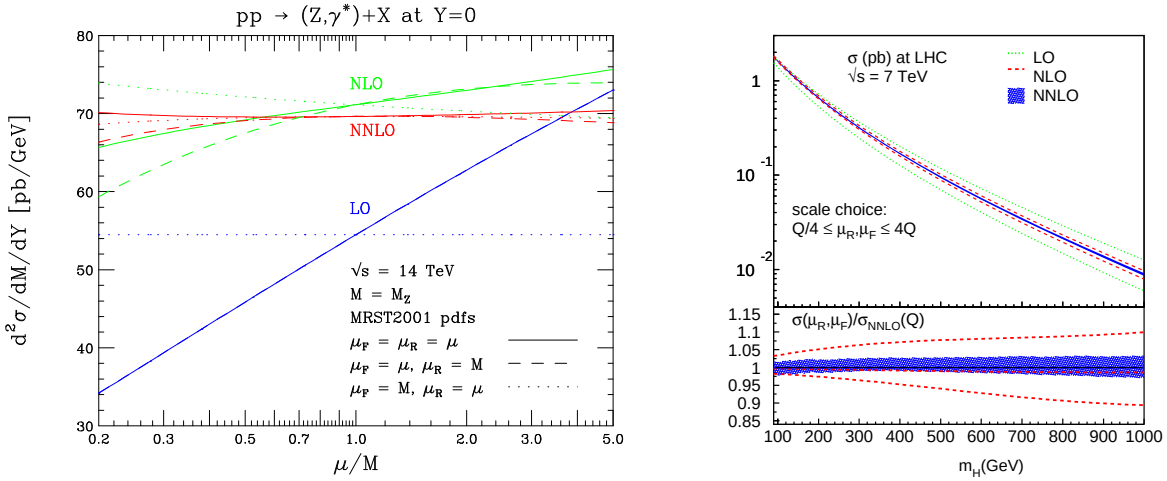

Figure 10: Examples of improvement in the predictions of processes at LHC in going from LO to NNLO. On the left, scale dependence of the predictions for Z/γ^* production (at $y = 0$) at the LHC14, at fixed order [25]. On the right, Higgs production at the LHC7 via VBF [26] as a function of the Higgs mass. The bands are obtained by independent scale variation in the interval $Q/4 \leq \mu_F, \mu_R \leq 4Q$, Q being the virtuality of the W, Z fusing into the Higgs. In both cases the perturbative expansion behaves extremely well and NNLO predictions overlap with those at LO and NLO and display a much smaller residual uncertainty.

(fully inclusive) distribution, which can be parametrized in terms of only two variables[8], the rapidity y_H and the transverse momentum p_H^T. At LO (referred to the total cross section), the Higgs can be boosted in the forward or backward directions in the lab system, $y_H = \frac{1}{2}\log\frac{x_1}{x_2}$, yet it has always $p_H^T = 0$, i.e. the distribution in p_H^T is a delta function centered at $p_H^T = 0$. At NLO (again referred to the total cross section), $2 \to 2$ diagrams enter in the calculation and the Higgs can have a non-zero p_H^T. Since at any point in phase space with $p_H^T \neq 0$ this is the first non-zero contribution, the observable p_H^T of the Higgs is only at LO. In other words if we want to know the p_H^T distribution of the Higgs at NLO over all phase space, we need at least a NNLO prediction for the cross section. Another way of thinking about it is to ask oneself what kind of diagrams are present in the calculation for that observable in a given area of the phase space: if there are only tree-level diagrams then the observable is LO. It is important when working with NLO codes to always think about what kind of observables are actually predicted at NLO, what at LO and what not even at LO. Again, a NNLO computation for the total cross section for $pp \to H + X$, gives NNLO information on the Higgs rapidity distribution, NLO for the Higgs p_H^T and $pp \to H + 1$-jet observables, LO for $pp \to H + 2$-jets observables and the structure of the jet in $H + 1$-jet events and no information at all on $pp \to H + 3$-jets observables. In short, a fixed-order computation can only make predictions for a finite number of observables, typically with a rather limited number of resolved partons and a very small number of unresolved ones, i.e. just one for a NLO computation and up to two for a NNLO computation. This is the first main limitation of a fixed-order computation. However, it is not the only one.

Consider again the p_H^T distribution of the Higgs as predicted by a NLO computation for the total cross section, Fig. 11. This curve can be easily obtained using the expressions in four dimensions of Eqs. (42,47,52), performing the integration over the polar angle together with the PDF's via a Monte-Carlo method and plotting it point-by-point during the integration. The p_H^T distribution is divergent in $p_H^T = 0$ as expected from soft and beam-collinear emissions. As we have learnt such divergences are proportional to $\delta(1-z)$ where z is the fraction of parton-parton energy taken by the Higgs and are cancelled by the virtual contributions, all of which reside in $p_T = 0$. So the cancellation between real and virtual contributions, all of it happens in the first bin of the histogram. How do we interpret such

[8] We do not consider the azimuthal angle ϕ, because for symmetry reasons can only lead to a uniform distribution

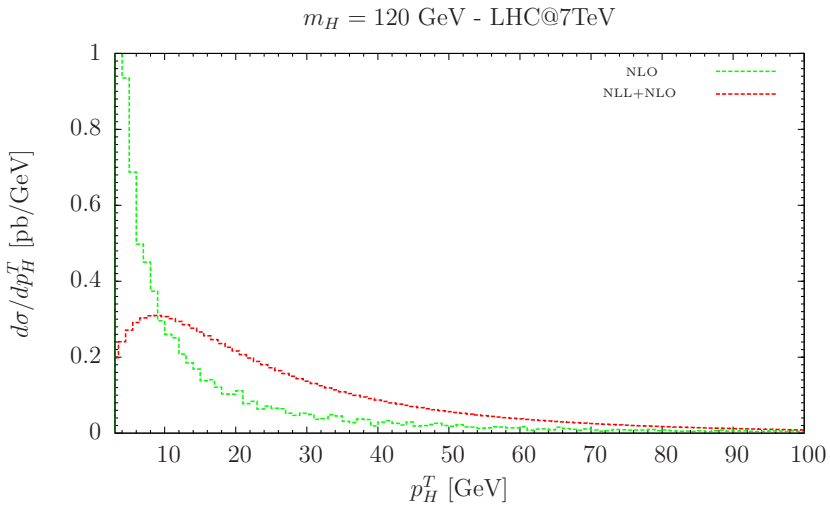

Figure 11: Higgs p_H^T spectrum for a Higgs of $m_H = 120$ GeV at the LHC7. The labeling NLO and NLL+NLO refer to the total cross section. The curves are normalized to the same value (=total cross section is the same). The green curve is just a LO prediction for the p_H^T of the Higgs. The logarithmic divergence at $p_H^T \to 0$ is cancelled by the negative infinite virtual contributions at $p_H^T = 0$ (not shown!). The resummed prediction (red curve) features a "physical" smooth behavior at small p_H^T. (The resummed prediction is obtained via HqT [27]).

weird distribution? A useful way is to think about the size of the bin of the distribution as our resolution scale: with a rather coarse binning there is no "going-to-infinity" and predictions are rather stable (this of course includes the total cross section which corresponds to using only one bin), while with thin binning, we start to be sensitive to low energy and virtual emissions which become increasingly important and are not included at all in a fixed-order approach. This is the case where resummed predictions come into rescue: one finds that the leading part of soft emissions (real and virtual) is universal, it can be considered at all orders and included by identifying the $\log$'s associated to it and exponentiating them. This can be done either at very high accuracy analytically yet fully inclusively or in a numerical and exclusive way at the leading log with a parton shower (which actually resums both soft and collinear enhancements). The result of including these effects analytically is shown in Fig. 11, red curve. In very crude words, the effect of the resummation is to spread the $\delta(p_T)$ of the virtual contributions over a range of a few tens of GeV with the effect of smoothing out the divergence and producing a "physical" distribution.

In summary, fixed-order calculations in perturbative QCD can be performed in a well-defined and quite simple framework, i.e. in the context of the factorization theorem. It is therefore possible to make predictions for inclusive quantities in hadron colliders, which can be systematically improved at the "only" price of an (exponential) increase in the complexity of the calculation. In practice, however, the use of fixed-order predictions is limited by several other important drawbacks. First, only processes with a few resolved partons can be calculated, while in practice we know that hundreds of hadrons can be produced in a single proton-proton interaction of which we are bound to ignore the details. Second, sharp infinities appear in the phase that do cancel between real and virtual contributions if inclusive enough observables are defined, yet lead to unphysical distributions in specific areas of the phase space and/or when the resolved partons become either soft or collinear. Such local positive and negative infinities are unphysical because they appear only due the artificial truncation of the perturbative expansion. Finally, the fact that plus and minus infinities appear locally in phase space also means that fixed order predictions beyond LO cannot be used as probability functions to generate events as distributed in nature. Parton showers, i.e. fully exclusive resummation, and their merging/matching with fixed-order predictions, provide an elegant and powerful way out to all the above limitations.

6 Beyond fixed-order predictions

As we have explicitly verified, fixed-order predictions have important limitations both of principle (areas of phase space and observables, such as jet substructure are poorly described, no hadrons but only partons) and in practice (no event simulation is possible). Fortunately, an alternative approach exists that is based on the fact that the IR structure, soft or collinear, of QCD is universal and contributions can be resummed at all orders. Last but not least, formulas that describe the emission of soft and collinear partons are amenable of a probabilistic interpretation and therefore not only it is possible to perform an explicit resummation but also to associate a full "history" to an hard scattering event, i.e., to associate to every event a full-fledged description of an high-energy event from the two initial protons to the final (possibly hundreds) of hadrons and leptons in the final state. In addition, in the latest years, enormous progress has been achieved in combining the accuracy of fixed-order predictions with the flexibility of parton showers. These methods are briefly presented here together with their applications to Higgs production. The short presentation below is adapted from Ref. [28]. The reader is also referred to [QCD:4.4] for further details, examples and references.

6.1 Parton Showers

Parton Showers (PS) are able to dress a given Born process with all the dominant (i.e. enhanced by collinear logarithms, and to some extent also soft ones) QCD radiation processes at all orders in perturbation theory. In particular, the dominant contributons, i.e. those given by the leading logarithms, coming from both real and virtual emissions are included. The cross section for the first (which is often also the hardest) emission in a shower reads:

$$\mathrm{d}\sigma^{\text{1st step}} = \mathrm{d}\Phi_B B(\Phi_B) \left[\Delta(p_\perp^{\min}) + \mathrm{d}\Phi_{R|B}\Delta(p_{\mathrm{T}}(\Phi_{R|B}))P(\Phi_{R|B})\right] , \tag{58}$$

where $\Delta(p_{\mathrm{T}})$ denotes the Sudakov form factor

$$\Delta(p_{\mathrm{T}}) = \exp\left[-\int \mathrm{d}\Phi_{R|B} P(\Phi_{R|B})\Theta(p_{\mathrm{T}}(\Phi_R) - p_{\mathrm{T}})\right] . \tag{59}$$

This Sudakov form factor can be understood as a no-emission probability of secondary partons down to a resolution scale of p_{T}. Here $P(\Phi_{R|B})$ is a process-independent universal splitting function that allows to write the PS approximation to the real cross section R^{PS}, typically given schematically by a product of the underlying Born-level term folded with a splitting kernel P

$$R^{\mathrm{PS}}(\Phi) = P(\Phi_{R|B})\, B(\Phi_B). \tag{60}$$

In this framework, $\Phi_{R|B}$ is often expressed in terms of three showering variables, like the virtuality t in the splitting process, the energy fraction of the splitting z and the azimuth ϕ. A very simple (and widely used) choice for the splitting function, is

$$P(\Phi_{R|B})d\Phi_{R|B} = \frac{\alpha_S(t)}{2\pi} P_{a\to bc}(z)\, \frac{d\phi}{2\pi}\, \frac{dt}{t}\, dz \tag{61}$$

where $P(z)$ are Altarelli-Parisi splitting functions on which any QCD amplitude factorisises in the collinear limit $b \parallel c$.

The above definition of the Sudakov form factor, guarantees that the square bracket in Eq. (58) integrates to unity, a manifestation of the probabilistic nature of the parton shower. Thus, integrating the shower cross section over the radiation variables yields the total cross section, given at LO by the Born amplitude. The corresponding radiation pattern consists of two parts: one given by the first term in the square bracket, where no further resolvable emission above the parton-shower cut-off $p_\perp^{\min}$ – typically of the order of 1 GeV – emerges, and the other given by the second term in the square bracket describing

the first emission, as determined by the splitting kernel. It is important to stress that the real-emission cross section in a PS generator is only correct in the small angle and/or soft limit, where $R^{\rm PS}$ is a reliable approximation of the complete matrix element.

After the 1st step the process is repeated using the new configuration as the Born one.

While rather crude, the PS approximation is a very powerful one, due mainly to the great flexibility and simplicity in the implementation of $2 \to 1$ and $2 \to 2$ high-Q^2 processes. In addition, once augmented with a hadronisation model the simulation can easily provide a full description of a collision in terms of physical final states, i.e., hadrons, leptons and photons. In the current terminology a generic Monte Carlo generator mainly refers to such tools, the most relevant examples of are PYTHIA 6 and PYTHIA 8 [29, 30], HERWIG [31], HERWIG++ [32], and SHERPA [33]. A very clear and exhaustive presentation of parton shower generators can be found in Ref. [34].

6.2 Matrix-element merging (ME+PS)

In parton showers algorithms QCD radiation is generated in the collinear and soft approximation, using Markov chain techniques based on Sudakov form factors. Hard and widely separated jets are thus poorly described in this approach. On the other hand, tree-level fixed order amplitudes can provide reliable predictions in the hard region, while failing in the collinear and soft limits. To combine both descriptions and avoid double counting or gaps between samples with different multiplicity, an appropriate merging method is required.

Matrix-element merging [35] aims at correcting as many large-angle emissions as possible with the corresponding tree-level accurate prediction, rather than only *small-angle* accurate. This is achieved by generating events up to a given (high) multiplicity using a matrix-element generator, with some internal jet-resolution parameter $Q_{\rm cut}$ on the jet separation, such that practically all emissions above this scale are described by corresponding tree-level matrix elements. Their contributions are corrected for running-coupling effects and by Sudakov form factors. Radiation below $Q_{\rm cut}$ on the other hand is generated by a parton-shower program, which is required to veto radiation with separation larger than $Q_{\rm cut}$. As far as the hardest emission is concerned, matrix-element merging is as accurate as matrix-element corrections (when these are available) or NLO+PS. Since they lack NLO virtual corrections, however, they do not reach NLO accuracy for inclusive quantities. Nevertheless, they are capable to achieve leading-order accuracy for multiple hard radiation, beyond the hardest only, while NLO+PS programs, relying on the parton shower there are only accurate in the collinear and/or soft limit for these quantities.

Several merging schemes have been proposed, which include the CKKW scheme [35–37] and its improvements [38, 39], the MLM matching [40], and the k_T-MLM variation [41]. The MLM schemes have been implemented in several matrix element codes such as ALPGEN [22], MADGRAPH [23], through interfaces to PYTHIA/HERWIG, while SHERPA [33] and HERWIG++ [32] have adopted the CKKW schemes and rely on their own parton showers. In Ref. [42] a detailed, although somewhat outdated description of each method has been given and a comparative study has been performed.

6.3 NLO+PS in a nutshell

Several proposals have been made for the full inclusion of complete NLO effects in PS generators. At this moment, only two of them have reached a mature enough stage to be used in practice: MC@NLO [43] and POWHEG [44]. Both methods correct – in different ways – the real-emission matrix element to achieve an exact tree-level emission matrix element, even at large angle. As we have seen in the previous subsection, this is what is also achieved with matrix-element corrections in parton showers, at least for the simplest processes listed earlier. This, however, is not sufficient for the NLO accuracy, since the effect of virtual corrections also needs to be included. In both methods, the real-emission cross section is split into a singular and non-singular part, $R = R^s + R^f$. One then computes the total NLO inclusive

cross section, excluding the finite contribution, at fixed underlying Born kinematics, defined as

$$\bar{B}^s = B(\Phi_B) + \left[V(\Phi_B) + \int \mathrm{d}\Phi_{R|B} R^s(\Phi_{R|B}) \right] , \tag{62}$$

and uses the formula

$$\mathrm{d}\sigma^{\mathrm{NLO+PS}} = \mathrm{d}\Phi_B \bar{B}^s(\Phi_B) \left[\Delta^s(p_\perp^{\min}) + \mathrm{d}\Phi_{R|B} \frac{R^s(\Phi_R)}{B(\Phi_B)} \Delta^s(p_{\mathrm{T}}(\Phi)) \right] + \mathrm{d}\Phi_R R^f(\Phi_R) \tag{63}$$

for the generation of the events. In this formula, the term $\bar{B}$ can be understood as a local K-factor reweighting the soft matrix-element correction part of the simulation. Clearly, employing the fact that the term in the first square bracket integrates to unity, as before, the cross section integrates to the full NLO cross section.

In MC@NLO one chooses R^s to be identically equal to the term $B \otimes P$ that the PS generator employs to generate emissions. Within MC@NLO, n-body events are obtained using the $\bar{B}^s$ function, and then fed to the PS, which will generate the hardest emission according to Eq. (62). These are called $\mathcal{S}$ events in the MC@NLO language. An appropriate number of events are also generated according to the R^f cross section, and are directly passed to the PS generator. These are called $\mathcal{H}$ events. In MC@NLO, $R^f = R - R^s$ is not positive definite, and it is thus necessary to generate negative weighted events in this framework. A library of MC@NLO Higgs processes (gluon fusion, vector-boson associated production, and charged Higgs associated with top) is available at Ref. [45], which is interfaced to HERWIG and HERWIG++. A fully automatized approach, AMC@NLO [46] implemented in the MADGRAPH framework, is now available that allows to compute and combine all necessary ingredients (Born, real, virtual matrix elements plus counterterms) at the user's request.

In POWHEG, one chooses $R^s \leq R$, and in many cases even $R^s = R$, so that the finite cross section R^f vanishes. In this case, the hardest emission is generated within POWHEG itself, and the process is passed to the parton shower only after the hardest radiation is generated. Positive weighted events are obtained, since R^f can always be chosen to be positive definite. In all cases the chosen R^s has exactly the same singularity structure as R, so that R^f always yield a finite contribution to the cross section. Implementations of Higgs production processes with the POWHEG method are available in HERWIG++ [47], in the POWHEGBOX [48] (interfaced to both HERWIG and PYTHIA) and recently in SHERPA [49].

6.4 Improved descriptions of Higgs production

Being of primary importance, Higgs kinematic distributions are now quite well predicted and also available via public codes such as ResBos [50] and HqT [27, 51]. Differential p_H^T distributions accurate to LO yet featuring the exact bottom- and top-quarks mass loop dependence (and therefore can be used also for predictions of scalar Higgs in BSM) can be obtained via HIGLU [52] as well as via HPro [53]. However, in experimental analyses, it is also crucial to get as precise predictions as possible for exclusive observables that involve extra jets, such as the jet p_T spectra and the jet rates, at both parton and hadron level. To optimize the search strategies and in particular to curb the very large backgrounds, current analyses both at Tevatron and at the LHC select 0-,1- and 2-jet events and perform independent analyses on each sample. The final systematic uncertainties are effected by both the theoretical and experimental ones of such a jet-bin based separation. In the HEFT, fully exclusive parton- and hadron-level calculations can now be performed by Parton Shower (PS) programs or with NLO QCD codes matched with parton showers: via the MC@NLO and POWHEG methods. Beyond the HEFT, fully exclusive predictions ME+PS and NLO+PS techniques has become available only recently [54, 55]. The reason is that one needs to compromise between the validity of HEFT and the complexity of higher loop calculations.

Fig. 12 shows a comparison of the predictions of the p^T of the Higgs at LHC7 as obtained in HEFT from:

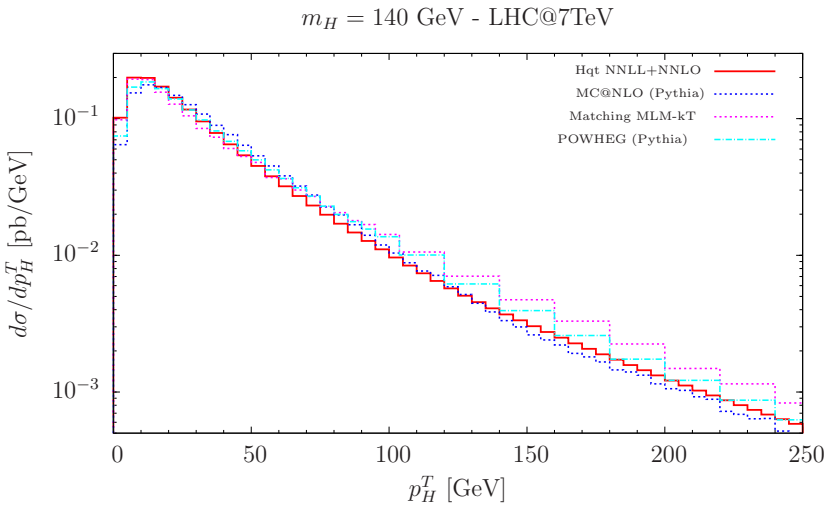

whe

Figure 12: Higgs p_H^T spectrum for a Higgs of $m_H = 140$ GeV as predicted by a series of improved predictions: NNLL+NNLO resummed (red solid), MC@NLO + Pythia (blue dashes), matrix-element + Pythia merged results (magenta dashes), POWHEG + Pythia (cyan dashes). All predictions display similar features, i.e. a peak between 10-20 GeV and a similar shape at high-p_H^T with differences that lie within their respective uncertainties (not shown).

– a full analytical resummation at NNLL;
– MC@NLO (w/ PYTHIA);
– ME+PS merging (MADGRAPH+PYTHIA);
– POWHEG (w/ PYTHIA).

We first stress (again) that this observable which is at NLO at high-p^T only in the Hqt predictions. The ME+PS approach is built to be LO for all observables, while MC@NLO and POWHEG predictions are based on the NLO calculation for the total cross section, the same performed in these notes. Notwidthstanding we see that given the expected uncertainties which are quite large above all at high-p^T the shapes are in substantial agreement both in the low and high-p^T ranges. In Fig. 13 the p^T distributions for the first and second jets are shown comparing the ME+PS prediction based on the HEFT and one with the full top-mass depedence and PYTHIA. Even in this case the agreeement between the various approaches is extremely good for a light Higgs. For a very heavy Higgs difference in the p_T distributions of the extra jets become visibile at quite a high p^T, a region not very relevant phenomenologically.

7 Conclusions

Progress in the field of QCD predictions for the LHC in the form of MC tools usable by both theorists and experimentalists has made tremendous progress in the last years. It is fair to say that we are now able (or close to be able in some specific very challenging cases) to compute automatically or semi-automatically any interesting cross section for Standard Model and Beyond processes at NLO accuracy and interface it with parton shower programs for event generation. In the LHC era the lowest acceptable accuracy for any serious phenomenological and experimental study is via an NLO event generator. LHC precision physics is now at NNLO in QCD and NLO in EW. Any physicist interested in making discoveries at the LHC needs to be familiar with the ideas, the physics and the reach of the current QCD simulation tools.

To this aim, we have considered $pp \to H + X$ as a case study. We have illustrated how accurate and useful predictions for cross sections and other observables can be obtained in QCD, starting from the calculation of Born amplitude (at one loop) and the corresponding hadronic cross section. We have

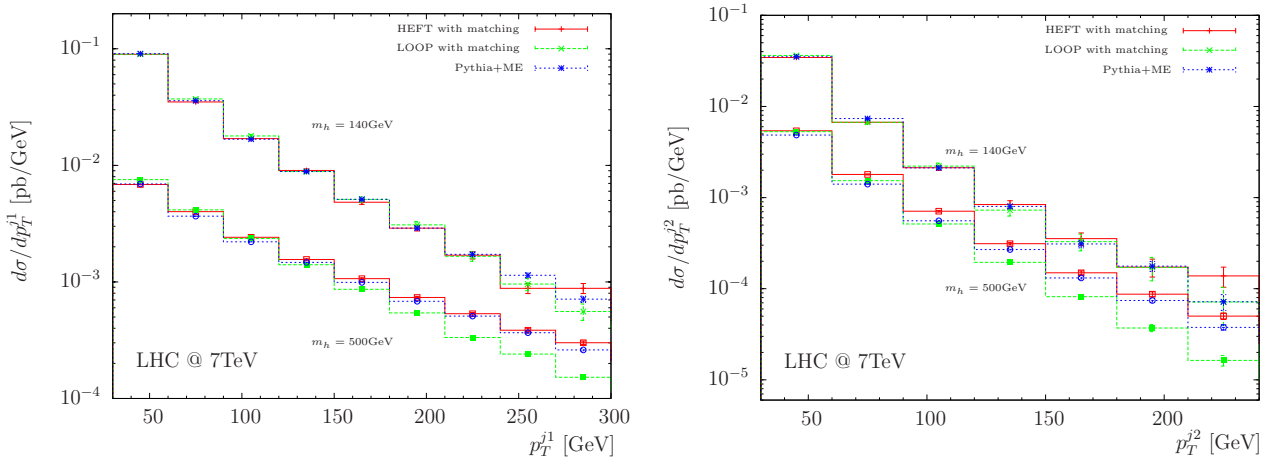

Figure 13: Jet p_T distributions for associated jets in gluon fusion production of $m_H = 140\,\text{GeV}$ and $m_H = 500\,\text{GeV}$ Higgs bosons at 7 TeV LHC.

then considered Higgs production at NLO in the HEFT and discussed the limitations of fixed-order predictions. Finally, we have briefly discussed how fully exclusive predictions are obtained with modern tools, that allow to reach the accuracy of NLO predictions together with the full exclusivity of a parton shower approach.

Appendix

Splitting functions and collinear counterterms

We define the 4-dimensional splitting functions as in (4.94) of the ESW book:

$$P_{qq}(z) = C_F\, p_{qq}(z) = C_F \left[\frac{1+z^2}{(1-z)_+} + \frac{3}{2}\delta(1-z)\right] \tag{64}$$

$$P_{qg}(z) = T_R\, p_{qg}(z) = T_R \left[z^2 + (1-z)^2\right] \tag{65}$$

$$P_{gq}(z) = C_F\, p_{gq}(z) = C_F \left[\frac{1+(1-z)^2}{z}\right] \tag{66}$$

$$P_{gg}(z) = C_A\, p_{gg}(z) = 2C_A \left[\frac{z}{(1-z)_+} + \frac{1-z}{z} + z(1-z)\right] + b_0\, \delta(1-z)\,, \tag{67}$$

where $b_0 = 11/6\, C_A - 2n_f T_F/3$. We also define the following quantities as the extension of the splitting functions in d-dimensions:

$$P_{ij}^{\rm d}(z) = P_{ij}(z) + \epsilon P_{ij}^{\epsilon}(z) \tag{68}$$

where

$$P_{qq}^{\epsilon}(z) = C_F\, p_{qq}^{\epsilon}(z) = -C_F(1-z) \tag{69}$$

$$P_{qg}^{\epsilon}(z) = T_R\, p_{qg}^{\epsilon}(z) = -T_R 2z(1-z) \tag{70}$$

$$P_{gq}^{\epsilon}(z) = C_F\, p_{gq}^{\epsilon}(z) = -C_F z \tag{71}$$

$$P_{gg}^{\epsilon}(z) = 0 \tag{72}$$

factorisation of the collinear divergences is performed through the addition of the following counterterm for each parton in the initial state:

$$\sigma_{\rm c.t.}^{\rm CDR} = \sigma_0^{\rm CDR}\ \frac{\alpha_S}{2\pi}\left[\left(\frac{\mu^2}{\mu_F^2}\right)^{\epsilon} \frac{c_\Gamma}{\epsilon} P_{ij}(z)\right] \tag{73}$$

where $\sigma_0^{\rm SCHEME}$ is the LO cross section and its value depends on the scheme (see the example for Drell-Yan)]. In CDR, when there is a collinear divergence, the cross section behaves as

$$\sigma_R^{\rm coll} \sim -\frac{1}{\epsilon} P_{ij}^{\rm d}(z) \sigma_0^{\rm CDR} + \text{other terms}\,. \tag{74}$$

Adding the counterterm (73), leaves a finite part

$$\sigma_R^{\overline{\rm MS}} \sim -P_{ij}^{\epsilon}(z)\ (\sigma_0^{\rm CDR}|_{\epsilon\to 0}) + \text{other terms}\,. \tag{75}$$

Bibliography

[1] R. K. Ellis, W. J. Stirling, and B. Webber, "QCD and collider physics," *Camb.Monogr.Part.Phys.Nucl.Phys.Cosmol.*, vol. 8, pp. 1–435, 1996.

[2] M. L. Mangano, "Introduction to QCD," *http://cdsweb.cern.ch/record/454171/files/open-2000-255.pdf*, no. CERN-OPEN-2000-255, 1999.

[3] P. Nason, "Introduction to QCD," *http://doc.cern.ch/cernrep/1998/98-03/98-03.html*, vol. C9705251, pp. 94–149, 1997.

[4] G. P. Salam, "Perturbative QCD for the LHC," *PoS*, vol. ICHEP2010, p. 556, 2010.

[5] H. Georgi, S. Glashow, M. Machacek, and D. V. Nanopoulos, "Higgs Bosons from Two Gluon Annihilation in Proton Proton Collisions," *Phys.Rev.Lett.*, vol. 40, p. 692, 1978.

[6] S. Dawson, "Radiative corrections to Higgs boson production," *Nucl.Phys.*, vol. B359, pp. 283–300, 1991.

[7] A. Djouadi, M. Spira, and P. Zerwas, "Production of Higgs bosons in proton colliders: QCD corrections," *Phys.Lett.*, vol. B264, pp. 440–446, 1991.

[8] D. Graudenz, M. Spira, and P. Zerwas, "QCD corrections to Higgs boson production at proton proton colliders," *Phys.Rev.Lett.*, vol. 70, pp. 1372–1375, 1993.

[9] M. Spira, A. Djouadi, D. Graudenz, and P. Zerwas, "Higgs boson production at the LHC," *Nucl.Phys.*, vol. B453, pp. 17–82, 1995.

[10] R. V. Harlander and W. B. Kilgore, "Next-to-next-to-leading order Higgs production at hadron colliders," *Phys.Rev.Lett.*, vol. 88, p. 201801, 2002.

[11] C. Anastasiou and K. Melnikov, "Higgs boson production at hadron colliders in NNLO QCD," *Nucl.Phys.*, vol. B646, pp. 220–256, 2002.

[12] V. Ravindran, J. Smith, and W. L. van Neerven, "NNLO corrections to the total cross-section for Higgs boson production in hadron hadron collisions," *Nucl.Phys.*, vol. B665, pp. 325–366, 2003.

[13] R. V. Harlander, H. Mantler, S. Marzani, and K. J. Ozeren, "Higgs production in gluon fusion at next-to-next-to- leading order QCD for finite top mass," *Eur. Phys. J.*, vol. C66, pp. 359–372, 2010.

[14] A. Pak, M. Rogal, and M. Steinhauser, "Finite top quark mass effects in NNLO Higgs boson production at LHC," *JHEP*, vol. 02, p. 025, 2010.

[15] R. V. Harlander, F. Hofmann, and H. Mantler, "Supersymmetric Higgs production in gluon fusion," *JHEP*, vol. 02, p. 055, 2011.

[16] A. Pak, M. Rogal, and M. Steinhauser, "Production of scalar and pseudo-scalar Higgs bosons to next-to-next-to-leading order at hadron colliders," *JHEP*, vol. 1109, p. 088, 2011. * Temporary entry *.

[17] M. R. Whalley, D. Bourilkov, and R. C. Group, "The Les Houches Accord PDFs (LHAPDF) and Lhaglue," 2005.

[18] S. Catani and M. Seymour, "A General algorithm for calculating jet cross-sections in NLO QCD," *Nucl.Phys.*, vol. B485, pp. 291–419, 1997.

[19] S. Frixione, Z. Kunszt, and A. Signer, "Three jet cross-sections to next-to-leading order," *Nucl.Phys.*, vol. B467, pp. 399–442, 1996.

[20] M. L. Mangano and S. J. Parke, "Multi-Parton Amplitudes in Gauge Theories," *Phys. Rept.*, vol. 200, pp. 301–367, 1991.

[21] L. J. Dixon, "Calculating scattering amplitudes efficiently," 1996.

[22] M. L. Mangano, M. Moretti, F. Piccinini, R. Pittau, and A. D. Polosa, "ALPGEN, a generator for hard multiparton processes in hadronic collisions," *JHEP*, vol. 0307, p. 001, 2003.

[23] J. Alwall, M. Herquet, F. Maltoni, O. Mattelaer, and T. Stelzer, "MadGraph 5 : Going Beyond," *JHEP*, vol. 1106, p. 128, 2011.

[24] S. Catani and M. Grazzini, "An NNLO subtraction formalism in hadron collisions and its application to Higgs boson production at the LHC," *Phys. Rev. Lett.*, vol. 98, p. 222002, 2007.

[25] C. Anastasiou, L. J. Dixon, K. Melnikov, and F. Petriello, "High precision QCD at hadron colliders: Electroweak gauge boson rapidity distributions at NNLO," *Phys.Rev.*, vol. D69, p. 094008, 2004.

[26] P. Bolzoni, F. Maltoni, S.-O. Moch, and M. Zaro, "Vector boson fusion at NNLO in QCD: SM Higgs and beyond," *Phys.Rev.*, vol. D85, p. 035002, 2012. 56 pages.

[27] D. de Florian, G. Ferrera, M. Grazzini, and D. Tommasini, "Transverse-momentum resummation: Higgs boson production at the Tevatron and the LHC," *JHEP*, vol. 11, p. 064, 2011.

[28] S. Dittmaier *et al.*, "Handbook of LHC Higgs Cross Sections: 1. Inclusive Observables," 2011. Long author list - awaiting processing.

[29] T. Sjostrand, S. Mrenna, and P. Z. Skands, "PYTHIA 6.4 Physics and Manual," *JHEP*, vol. 0605, p. 026, 2006.

[30] T. Sjostrand, S. Mrenna, and P. Z. Skands, "A Brief Introduction to PYTHIA 8.1," *Comput.Phys.Commun.*, vol. 178, pp. 852–867, 2008.

[31] G. Corcella, I. Knowles, G. Marchesini, S. Moretti, K. Odagiri, *et al.*, "HERWIG 6: An Event generator for hadron emission reactions with interfering gluons (including supersymmetric processes)," *JHEP*, vol. 0101, p. 010, 2001.

[32] M. Bahr, S. Gieseke, M. Gigg, D. Grellscheid, K. Hamilton, *et al.*, "Herwig++ Physics and Manual," *Eur.Phys.J.*, vol. C58, pp. 639–707, 2008. 143 pages, program and additional information available from http://projects.hepforge.org/herwig.

[33] T. Gleisberg, S. Hoeche, F. Krauss, A. Schalicke, S. Schumann, *et al.*, "SHERPA 1. alpha: A Proof of concept version," *JHEP*, vol. 0402, p. 056, 2004.

[34] A. Buckley, J. Butterworth, S. Gieseke, D. Grellscheid, S. Hoche, *et al.*, "General-purpose event generators for LHC physics," *Phys.Rept.*, vol. 504, pp. 145–233, 2011.

[35] S. Catani, F. Krauss, R. Kuhn, and B. Webber, "QCD matrix elements + parton showers," *JHEP*, vol. 0111, p. 063, 2001.

[36] F. Krauss, "Matrix elements and parton showers in hadronic interactions," *JHEP*, vol. 0208, p. 015, 2002.

[37] L. Lonnblad, "Correcting the color dipole cascade model with fixed order matrix elements," *JHEP*, vol. 0205, p. 046, 2002.

[38] S. Hoeche, F. Krauss, S. Schumann, and F. Siegert, "QCD matrix elements and truncated showers," *JHEP*, vol. 0905, p. 053, 2009.

[39] K. Hamilton, P. Richardson, and J. Tully, "A Modified CKKW matrix element merging approach to angular-ordered parton showers," *JHEP*, vol. 0911, p. 038, 2009.

[40] M. L. Mangano, M. Moretti, and R. Pittau, "Multijet matrix elements and shower evolution in hadronic collisions: $Wb\bar{b}$ + n jets as a case study," *Nucl.Phys.*, vol. B632, pp. 343–362, 2002.

[41] J. Alwall, S. de Visscher, and F. Maltoni, "QCD radiation in the production of heavy colored particles at the LHC," *JHEP*, vol. 0902, p. 017, 2009.

[42] J. Alwall, S. Hoche, F. Krauss, N. Lavesson, L. Lonnblad, *et al.*, "Comparative study of various algorithms for the merging of parton showers and matrix elements in hadronic collisions,"

Eur.Phys.J., vol. C53, pp. 473–500, 2008.

[43] S. Frixione and B. R. Webber, "Matching NLO QCD computations and parton shower simulations," *JHEP*, vol. 0206, p. 029, 2002.

[44] P. Nason, "A New method for combining NLO QCD with shower Monte Carlo algorithms," *JHEP*, vol. 0411, p. 040, 2004.

[45] S. Frixione, F. Stoeckli, P. Torrielli, B. R. Webber, and C. D. White, "The MCaNLO 4.0 Event Generator," 2010.

[46] R. Frederix, S. Frixione, V. Hirschi, F. Maltoni, R. Pittau, *et al.*, "Scalar and pseudoscalar Higgs production in association with a top-antitop pair," *Phys.Lett.*, vol. B701, pp. 427–433, 2011.

[47] K. Hamilton, P. Richardson, and J. Tully, "A Positive-Weight Next-to-Leading Order Monte Carlo Simulation for Higgs Boson Production," *JHEP*, vol. 0904, p. 116, 2009.

[48] S. Alioli, P. Nason, C. Oleari, and E. Re, "A general framework for implementing NLO calculations in shower Monte Carlo programs: the POWHEG BOX," *JHEP*, vol. 1006, p. 043, 2010.

[49] S. Hoche, F. Krauss, M. Schonherr, and F. Siegert, "Automating the POWHEG method in Sherpa," *JHEP*, vol. 1104, p. 024, 2011.

[50] C. Balazs, J. Huston, and I. Puljak, "Higgs production: A Comparison of parton showers and resummation," *Phys. Rev.*, vol. D63, p. 014021, 2001.

[51] G. Bozzi, S. Catani, D. de Florian, and M. Grazzini, "Transverse-momentum resummation and the spectrum of the Higgs boson at the LHC," *Nucl. Phys.*, vol. B737, pp. 73–120, 2006.

[52] U. Langenegger, M. Spira, A. Starodumov, and P. Trueb, "SM and MSSM Higgs Boson Production: Spectra at large transverse Momentum," *JHEP*, vol. 0606, p. 035, 2006.

[53] C. Anastasiou, S. Bucherer, and Z. Kunszt, "HPro: A NLO Monte-Carlo for Higgs production via gluon fusion with finite heavy quark masses," *JHEP*, vol. 0910, p. 068, 2009.

[54] J. Alwall, Q. Li, and F. Maltoni, "Matched predictions for Higgs production via heavy-quark loops in the SM and beyond," *Phys. Rev.*, vol. D85, p. 014031, 2012.

[55] E. Bagnaschi, G. Degrassi, P. Slavich, and A. Vicini, "Higgs production via gluon fusion in the POWHEG approach in the SM and in the MSSM," *JHEP*, vol. 02, p. 088, 2012.